

CFD Simulation of a Bag Filter for a 200MW Power Plant

Yukun Lv, Jiayi Yang* and Jing Wang

North China Electric Power University, Baoding, 071003, China

*Corresponding Author: Jiayi Yang. Email: markwood@foxmail.com

Received: 25 February 2020; Accepted: 22 September 2020

Abstract: The combustion of pulverized coal inevitably produces dust and other harmful substances. For these reasons, the optimization of de-dusting procedure and equipments is an aspect of crucial importance towards the final goal of making this source of energy more sustainable. In the present work, the behaviour of a “bag filter” is simulated using Computational Fluid Dynamics (CFD). More specifically, three possible approaches are used, differing with respect to the level of fidelity and the partial utilization of empirical data. The outcome of these simulations is mutually compared and finally discussed critically in the light of available experimental results.

Keywords: De-dusting; bag filter; computational fluid dynamics (CFD); simulation; empirical data

1 Introduction

With the continuous development of the economy, the lives of people are changing with each passing day and the demand for electricity is increasing [1]. Because of mature technology development, 200 MW units will remain important thermal power plant units in the future. Furthermore, 200 MW units will remain the main power source of many self-contained power plants [2]. However, the combustion of pulverised coal inevitably produces dust and other harmful substances; in particular, 200-MW units produce a considerable amount of dust during operation. Therefore, the dedusting equipment of the 200 MW units must be investigated to reduce the harm to human health.

The common supporting dedusting equipment of the 200 MW units includes a cyclone deduster, an electrostatic precipitator and a bag filter [3,4]. However, with the continuous improvement of the emission standards, the cyclone deduster and electrostatic precipitator do not often meet the emission requirements of particulate matter. The bag filter has attracted considerable research attention because of its high efficiency for dedusting ultra-fine particles, large capacity for flue gas treatment and simple installation and maintenance. However, during operation, the bag filter often affects the safe and economic operation of the unit due to its high resistance. Therefore, it is important to rapidly, directly and accurately analyse the overall resistance characteristics of the bag filters with the 200 MW units.

Many scholars have investigated the resistance generation mechanisms and control methods associated with bag filters. Ma [5] analysed the damage and failure of the filter bags and determined the high temperature of the flue gas, high NO_x content of the flue gas and high injection pressure to be the main



This work is licensed under a Creative Commons Attribution 4.0 International License, which permits unrestricted use, distribution, and reproduction in any medium, provided the original work is properly cited.

reasons for the increase in resistance. Kim et al. [6] determined that the effective filtration area of the pleated filter bag is approximately 50%–60% compared with that of the circular filter bag. Rachid et al. [7] investigated the influence of air humidity on the filtration performance of the bag filter and determined that the increase in bag resistance of the filter can be mainly attributed to the capillary condensation of water. Lu et al. [8] used two-phase flow to simulate the inside of the annular bag filter and determined that the filter bag and the outer dust layer were the main sources of resistance; thus, the usage of the annular bag had a positive effect on drag reduction. Park et al. [9] investigated the length of the bag filter and concluded that the non-uniformity of the flue gas velocity in the bag along the axial direction will increase rapidly when the length of the bag filter becomes greater than 10 m. Thus, the length of the bag filter should be less than 10 m. In their research on dust removal using a bag filter, Andersen et al. [10] proposed that reducing the throat diameter of the venturi jet pipe can reduce the reflux, improve the pulse pressure, improve the jet into the filter bag and reduce the resistance that can be attributed to the dust layer in the pulse jet dust bag filter. Nie [11] fabricated a ‘high-efficiency and low-resistance’ filter bag with an ultra-fine glass fibre high-density surface layer, thereby reducing the overall resistance of the bag filter to a certain extent. Geng et al. [12] designed the internal circulating electric heating system of the bag filter similar to that of the waste incineration power plant, alleviating the condensation and acid corrosion of the waste incinerator to a certain extent. Yin et al. [13] reported that the strength and strength distribution of ash removal with respect to the same row of filter bags are affected by the distribution of air momentum flux at the outlet of each nozzle and designed a spray pipe with improved ash removal effect, reducing the thickness of the dust layer on the outside of the filter bag to a certain extent and improving the overall drag reduction effect of the filter bag.

The internal velocity and pressure-field characteristics of the filter bag must be analysed because only some studies have investigated simple numerical simulation methods with respect to the resistance characteristics of the bag filter matched with the 200 MW unit. Based on the existing studies on the resistance generation mechanisms and control methods, the usage of SolidWorks and computational fluid dynamics (CFD) has been proposed to conduct numerical analysis and explore the global simulation method, local simulation method and local simulation plus the refined empirical number method to predict the overall resistance of the bag filter. Further, the methods that can be used to determine the overall resistance of the bag filter of the 200 MW units rapidly and accurately are provided. These methods can be used as reference to calculate the resistance of the bag filters matched with other capacity units.

2 Bag Filter and its Theoretical Introduction

2.1 Bag Filter

In the 1950s, the world was dominated by electrostatic precipitators. However, in the 1970s, with the increasingly strict requirements of some developed countries for environmental protection, the bag filter was widely utilised by all the countries in the world because of its high dust removal rate in case of ultra-fine particles.

The overall pressure loss (overall resistance) of the bag filter is an important index based on which its performance can be evaluated [14,15]. The greater the overall pressure loss, the greater will be the energy consumption of the induced draft fan. Thus, the overall pressure loss is also an index that can be used to measure the energy consumption and operating cost of the dedusting equipment [16].

The analysis of the overall resistance of the bag filter is commonly divided into calculation, simulation and testing. During calculation, the number of filter bags, permeability coefficient, specific operating time, flue gas concentration, fibre layer thickness of the filter bags and other data must be determined and substituted into the empirical formula to obtain results. However, the economics of this method is poor. When simulating the numerical values, the overall model of the filter, internal filter bags and other fine structures must be established. The simplified method involves division into a large number of grids, with

small fault tolerance and low efficiency. During the test, considerable manpower and material resources have to be invested during the field survey because the test bag filters are often located far from each other. Thus, it is difficult to ensure timeliness and feasibility. To determine the overall resistance of the bag filter of the 200 MW units and save calculation resources, two methods have been proposed to analyse the resistance of the bag filter, including the simulation of a single filter bag and its shell and that of a single filter bag along with the experience value, which can save time and calculation resources.

2.2 Porous Media Model

In real life, the problem of porous media is often encountered, which is characterised by several geometric gaps. It is difficult to establish a real-life geometric model. This type of problem is usually simplified in CFD. The porous area is always simplified as a fluid area with increased resistance source, and the control equation is simplified as the momentum sink related to velocity [17,18]. The control equation can be expressed as follows:

$$S_i = - \left(\sum_{j=1}^3 Q_{ij} \mu v_j + \sum_{j=1}^3 C_{ij} \frac{1}{2} \rho |v| v_j \right) \quad (1)$$

where S_i is the source term of the momentum equation in the $I(x, y, z)$ direction, μ is the dynamic viscosity (Pa·s), $|v|$ is the velocity (m/s) and Q_{ij} and C_{ij} are the specified matrices. The first and second terms on the right side of the formula are the viscosity loss term and the inertia loss term, respectively.

In case of uniform media, the equation expressed in Formula (1) can be rewritten as follows:

$$S_i = - \left(\frac{\mu}{\alpha} v_i + C_2 \frac{1}{2} |v| v_i \right) \quad (2)$$

where α is the permeability (D), C_2 is the inertial resistance coefficient and the matrix Q in Formula (1) is $1/\alpha$.

The momentum sink acts on the fluid to produce a pressure gradient $\Delta P = -S_i \Delta n$ where Δn is the thickness of the porous medium.

3 Simulation Schemes of the Bag Filter

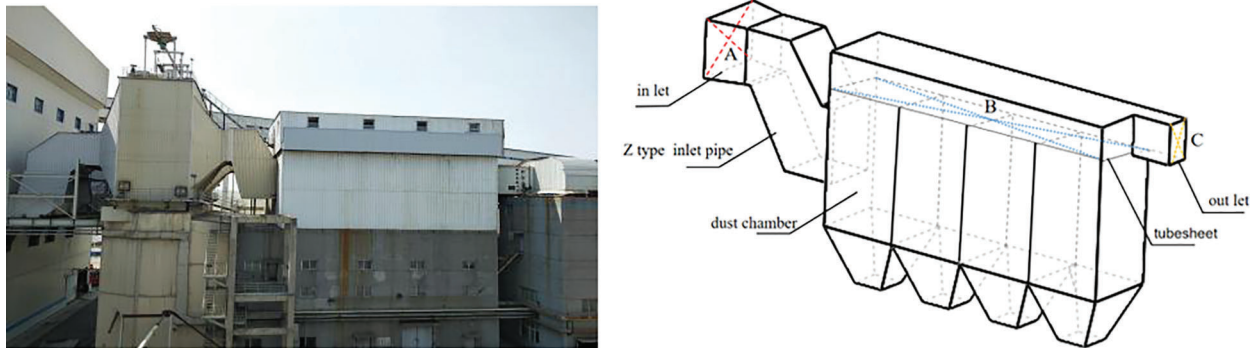
3.1 Scheme 1: Global Simulation Method

The bag filter matching unit #1 in a self-owned power plant is considered as an example. The filter bag in the equipment is blocked, hardened, corroded and damaged owing to air leakage and poor coal quality, which reduces the dedusting efficiency and increases the pressure loss, affecting the operational safety of the unit.

The structure and size of the matched bag filter are presented in Tab. 1. A complete model is built via SolidWorks by considering a 1:1 ratio. The actual appearance and model structures are shown in Fig. 1. A rectangular ‘bell mouth’ is installed at the inlet of the bag filter, and the pressure-measuring point A is located at the intersection of the diagonal (the red dotted line in Fig. 1) of the rectangular section. The flue gas flows through the Z-shaped air inlet pipe to enter the shell of the bag filter. The shell of the bag filter is divided into four chambers, numbered from the inlet as the first to fourth dedusting chambers. The dedusting chamber contains a rectangular tubesheet. The pressure-measuring point B is located at the intersection of the diagonal (blue dotted line in Fig. 1) of the tubesheet, and the pressure-measuring point C is located at the intersection of the diagonal (yellow dotted line in Fig. 1) of the rectangular section of the outlet. The static pressure difference between points A and C is approximately the difference between the static pressures of the inlet and outlet.

Table 1: Grid independence test of the bag filter

Grid density	7.456×10^6	8.504×10^6	9.439×10^6	9.804×10^6	10.106×10^6	10.374×10^6
Resistance of the inlet and outlet (Pa)	2785.43	2919.42	3257.33	3385.4	3385.4	3385.3

**Figure 1:** Appearance and model of the bag filter

A high-performance computer with the Opteron 6174 central processing unit (CPU) is used to divide the grid based on the mesh module in Workbench 16.0. The data shown in Tab. 1 are used to verify the independence of the grids. In Tab. 1, when the number of grids is greater than 9.804×10^6 , the resistance values of the inlet and outlet remain almost unchanged at the BMCR point. Thus, the number of grids used is approximately 9.8 million.

Then, the model is imported into Fluent, and the gravitational acceleration is set as 9.81 m/s^2 . The laminar model is selected when the resistance loss along the way is ignored.

The value of U of the unit is between 0.8 and 0.9 m/min under half-load conditions at the BMCR point. After calculating the hydraulic diameter based on the data of the rectangular section of the bag filter with the approximate rectangular channel shown in Tab. 2, the hydraulic diameter is substituted into the Reynolds number (Re) expressed in Formula (3). When the Re of the bag filter is between 1,925.3 and 2,166.04, a laminar flow can be observed. The governing equations of the laminar model include the mass conservation equation (Formula (4)) and the energy conservation equations (Formulas (5–7)) [19,20].

Table 2: Bag filter structure and size

Bell mouth/mm	Total length of the Z-type pipeline/mm	Front length of the Z-type pipe/mm	Back length of the Z-type pipe/mm	Z-type entrance angle/ $^\circ$	Single chamber of the bag filter/mm	Bottom length of the ash hopper/mm	Ash bucket angle/ $^\circ$	Number of filter rooms/each	Entrance/mm
4700×3500	6600	3170	970	120	$5040 \times 4695 \times 8300$	1970	69	4	4700×3500

Regardless of the influence of ash cleaning, the overall resistance of the filter bag and the dust layer after stable operation is converted into the internal porous zone. According to Formulas (1) and (2), the viscous and inertial resistance coefficients are $D = 4.84 \times 10^6$ and $C_2 = 5.57$, respectively. Finally, based on the commonly used numerical simulation methods [21,22], the standard wall is selected, the velocity inlet, pressure outlet and standard initialisation are set and the convergence is iteratively calculated to be approximately 40 h.

$$Re = \frac{UL}{\nu} \tag{3}$$

$$\frac{\partial \rho}{\partial t} + \frac{\partial(\rho u)}{\partial x} + \frac{\partial(\rho v)}{\partial y} + \frac{\partial(\rho w)}{\partial z} = 0 \tag{4}$$

$$\frac{\partial(\rho u)}{\partial t} + \frac{\partial(\rho uu)}{\partial x} + \frac{\partial(\rho uv)}{\partial y} + \frac{\partial(\rho uw)}{\partial z} = \frac{\partial}{\partial x} \left(\mu \frac{\partial u}{\partial x} \right) + \frac{\partial}{\partial y} \left(\mu \frac{\partial u}{\partial y} \right) + \frac{\partial}{\partial z} \left(\mu \frac{\partial u}{\partial z} \right) - \frac{\partial p}{\partial x} \tag{5}$$

$$\frac{\partial(\rho v)}{\partial t} + \frac{\partial(\rho vu)}{\partial x} + \frac{\partial(\rho vv)}{\partial y} + \frac{\partial(\rho vw)}{\partial z} = \frac{\partial}{\partial x} \left(\mu \frac{\partial v}{\partial x} \right) + \frac{\partial}{\partial y} \left(\mu \frac{\partial v}{\partial y} \right) + \frac{\partial}{\partial z} \left(\mu \frac{\partial v}{\partial z} \right) - \frac{\partial p}{\partial y} \tag{6}$$

$$\frac{\partial(\rho w)}{\partial t} + \frac{\partial(\rho wu)}{\partial x} + \frac{\partial(\rho wv)}{\partial y} + \frac{\partial(\rho ww)}{\partial z} = \frac{\partial}{\partial x} \left(\mu \frac{\partial w}{\partial x} \right) + \frac{\partial}{\partial y} \left(\mu \frac{\partial w}{\partial y} \right) + \frac{\partial}{\partial z} \left(\mu \frac{\partial w}{\partial z} \right) - \frac{\partial p}{\partial z} \tag{7}$$

where U is the flue gas filtration speed, m/s; L is the equivalent diameter; ν is the kinematic viscosity, m^2/s ; ρ is the density, kg/m^3 ; u , v and w are the components of filtration speed in the x , y and z directions, m/s and P is the pressure on the fluid microelement, Pa.

The simulation results of the static pressure difference between point AB, inlet and outlet under the three aforementioned conditions are shown in Fig. 2.

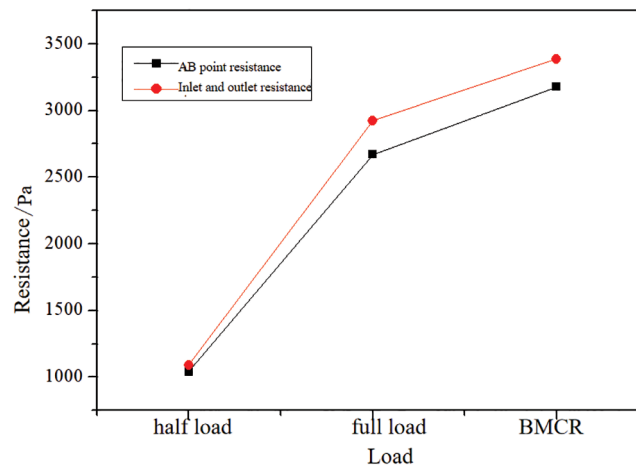


Figure 2: Statistics of the global simulation of the static pressure difference

3.2 Scheme 2: Local Simulation Method

The global simulation must be fully modelled, and a large number of grids must be divided. At the same time, the calculation associated with the global simulation is time-consuming and laborious. The local simulation method is adopted to simplify the simulation process and save time, i.e., only a single filter bag and its shell are modelled based on the real object. The total resistance can be obtained by adding the simulated pressure difference of a single filter bag and its shell under the corresponding working condition. The total resistance can be expressed as follows:

$$P = np_B + p_S \quad (8)$$

where n is the number of filter bags, pcs; p_B is the differential pressure of a single filter bag, Pa and p_S is the differential pressure of the shell, Pa.

The frictional drag is small, only (approximately 5.52×10^{-4} to 4.36×10^{-4} Pa). When the bag filter is running, Re is 1,925.3–2,166.04, the flue gas is in laminar flow and the friction resistance and differential pressure resistance on the leeward side of the filter bag can be ignored. The resistance from the inside of the filter bag to the outlet is less than that from the leeward side, and the bottom section is small. Thus, the following simplified assumptions can be obtained.

- 1) The filter bag used in the bag filter will not deform during operation.
- 2) The resistance loss along the way is ignored.
- 3) During operation, the flue gas is in laminar flow and the flow resistance is ignored.
- 4) The normal velocity of flue gas at the bottom and leeward side of the filter bag approaches 0, i.e., $\frac{\partial v}{\partial u} \rightarrow 0$.
- 5) After the stable operation of the unit, the thickness of the dust layer on the outside of the filter bag remains unchanged.

The simplified hypothetical process of the flue gas flowing through the filter bag is shown in Fig. 3A. The internal part of the filter bag is considered to be the porous media area. After the grid independence test (Tab. 3), approximately 1.5×10^4 grids are selected for the simulation; the remaining settings remain unchanged. The velocity plot of the axial section of the simulated filter bag is shown in Fig. 3B, and the static pressure plot is shown in Fig. 3C. The pressure differences between the inlet and outlet of a single filter bag are 0.646, 2.215 and 2.592 Pa under the half-load, full-load and BMCR conditions, respectively. Because there are 944 filter bags in the bag filter, the total resistance between the inlet and outlet of the bag filter is calculated using Formula (8) and determined to be 609.82, 2090.96 and 2446.85 Pa under half-load, full-load and BMCR conditions, respectively.

Further, the shell of the bag filter is modelled. Approximately 3 million grids are selected after the grid independence test (Tab. 4). Then, the laminar model is used again to calculate the pressure difference between point AB, inlet and outlet under the BMCR, full-load and half-load conditions. The plots of velocity and static pressure at the BMCR point are shown in Fig. 4.

The flue gas mainly affects the second dust collection chamber at the lower part of the shell. The resistance of the second and third chambers of the bag filter is large, which is the same as that observed with respect to the flow characteristics of the simulation using Method 1. The total resistance of the bag filter can be obtained using Formula (8) (Tab. 5).

The statistics show that the total simulation time of this method is only approximately 10 h and that the occupancy rate of the CPU is 30%–50%.

3.3 Scheme 3: Local Simulation Plus Refined Empirical Number Method

To satisfy the requirements of practical engineering prediction, a local simulation method is used to simulate the pressure difference of a single filter bag, which is multiplied by the total number of filter bags and added to the empirical number of the resistance of the shell of the bag filter matched with the 200-MW units. Thus, the total resistance can be approximately obtained.

Under normal conditions, the resistance of the shell of the bag filter is approximately considered to be its structural resistance. This generally includes the local resistance of the inlet and outlet, the frictional drag and the local resistance of the guide and baffle plates in the ash hopper. Generally, the resistance is between 200 and 500 Pa [23,24].

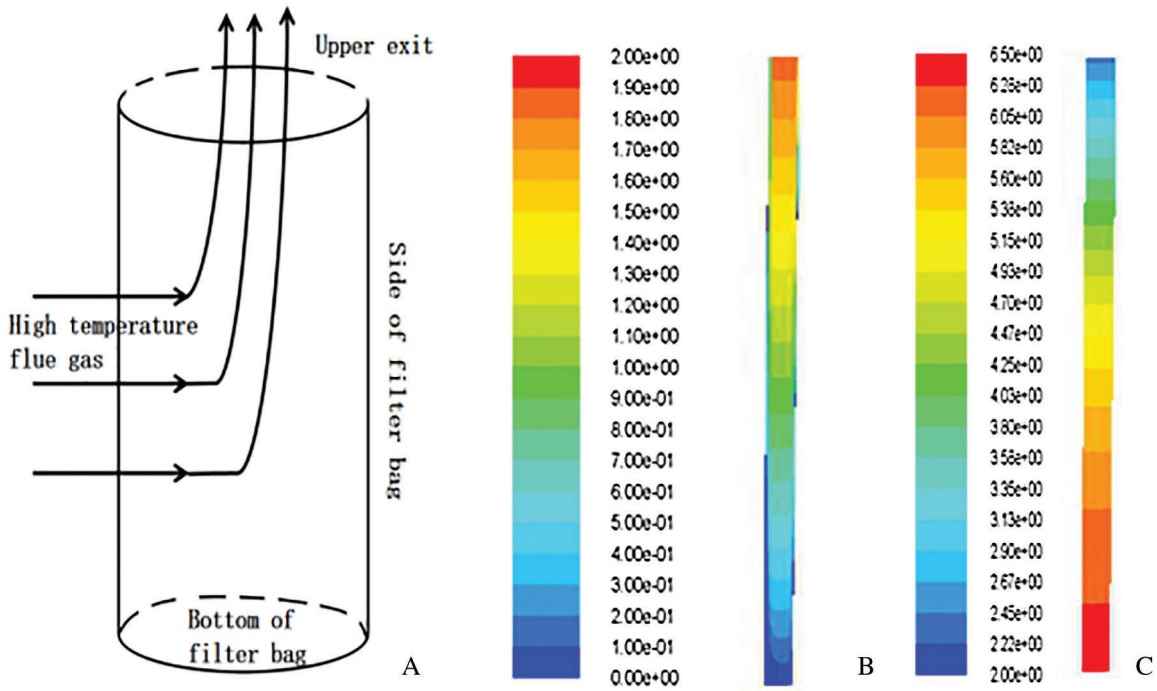


Figure 3: Schematic of the filter bag and its simulation

Table 3: Grid independence test of the filter bag

Grid density	10.23×10^4	13.37×10^6	15.24×10^6	17.01×10^6	18.074×10^6
Resistance of the inlet and outlet (Pa)	2.431	2.590	2.592	2.592	2.592

Table 4: Grid independence test of the shell

Grid density	2.48×10^6	2.88×10^6	3.07×10^6	3.24×10^6	3.51×10^6
Resistance of the inlet and outlet (Pa)	518.89	527.11	558.94	558.94	558.94

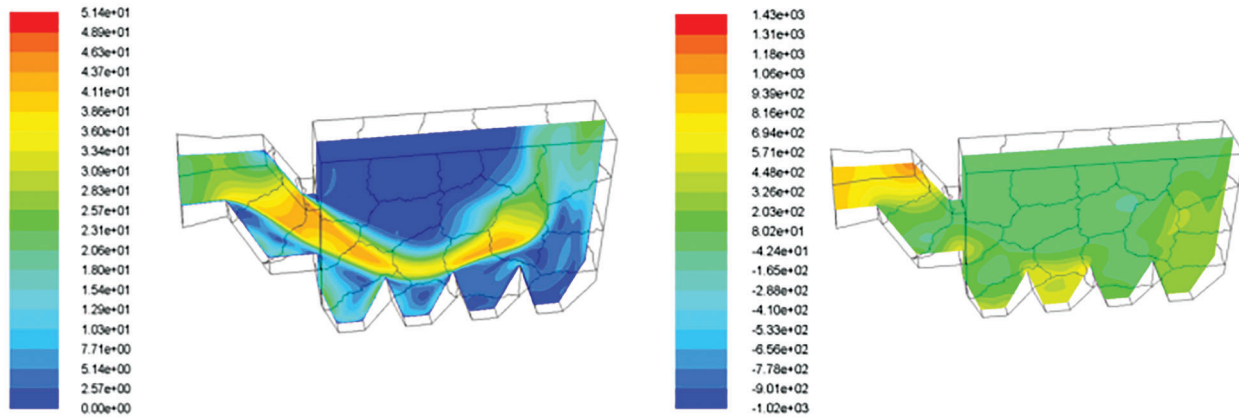


Figure 4: Plots of the shell velocity and static pressure at the BMCR point

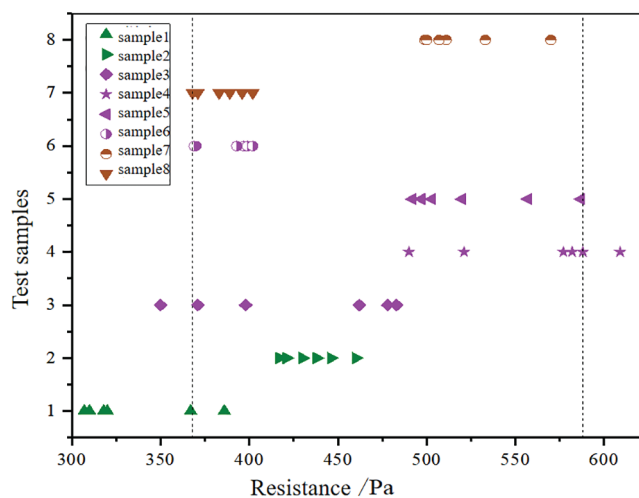
Table 5: Local simulation of the total resistance of the bag filter

Conditions	Half-load condition	Rated-load condition	BMCR condition
Resistance of the point AB (Pa)	877.86	2519.52	2907.75
Resistance of the inlet and outlet (Pa)	891.52	2600.25	3005.79

Eight representative bag filters of thermal power plants are selected as the test samples to further refine the empirical values of the shell resistance of the supporting bag filter of the 200-MW unit, and the units of these eight power plants are 200 MW.

The resistance (static pressure difference) of the shell was measured at the half-load, full-load and BMCR point according to GB 5468-1991 and GB/T 13931-2017 after the filter bag was removed using the TH880W microcomputer smoke (flue gas) parallel sampling instrument.

Then, the scatter plot is developed using the experimental data (Fig. 5). As shown in Fig. 5, only some data points can be observed outside the two dashed lines. In contrast, the data points are dense inside the two dashed lines. Therefore, after eliminating the data points outside the dashed lines, the shell resistance of the bag filter of the 200 MW unit is generally between 368 and 588 Pa. Thus, the refined range is reduced by 26.7% when compared with the original empirical values.

**Figure 5:** Distribution of the resistance of the shell of the bag filter

According to Formula (8), the value range of p_s is replaced by 368–588 Pa, the numerical simulation and calculation can be completed in 1 h and the CPU utilisation rate is not more than 18%. The value range of the total resistance P between the inlet and outlet under half-load, full-load and BMCR conditions can be obtained via simulation and calculation. The ranges of the total resistance under half-load, full-load and BMCR conditions are 977.82–1197.82, 2458.96–2678.96 and 2814.85–3034.85 Pa, respectively.

4 Comparative Verification Analysis

4.1 Method 1 and Actual Measurement

The resistance test value of the bag filter under half-load, full-load and BMCR conditions is compared with the global simulation value to verify the feasibility of the overall model (Fig. 6). According to the data

analysis presented in the figure, the deviation between the simulation result and the actual measured value is less than 9.1%, verifying the feasibility of the construction of the overall model [25–27].

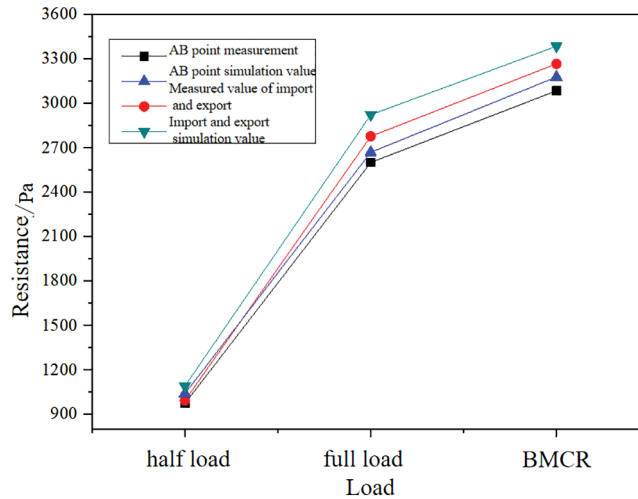


Figure 6: Statistics of the global simulation of the resistance of the bag filter and the measured value

4.2 Comparison of Different Methods

Fig. 7A presents the comparison of the value obtained using the local simulation method (Method 2) and the actual measured value. Fig. 7B shows the comparison of the value obtained using the local simulation plus refined empirical number method (Method 3) and the actual measured value. Fig. 7A shows that the simulated value obtained using Method 2 is slightly smaller than the actual measured value under the three working conditions regardless of point AB or the resistance between the inlet and outlet and because the overall resistance loss along the way and the disturbance resistance between the filter bags are ignored, and the maximum error is only 10.2%. Therefore, the correction coefficient ε is defined as the error caused by neglecting the secondary resistance when simulating a single filter bag and its shell. The value range of ε is from 5.7% to 10.2%. Thus, Formula (8) can be optimised and rewritten as Formula (9), and more accurate overall resistance values can be obtained using Formula (9) after simulation.

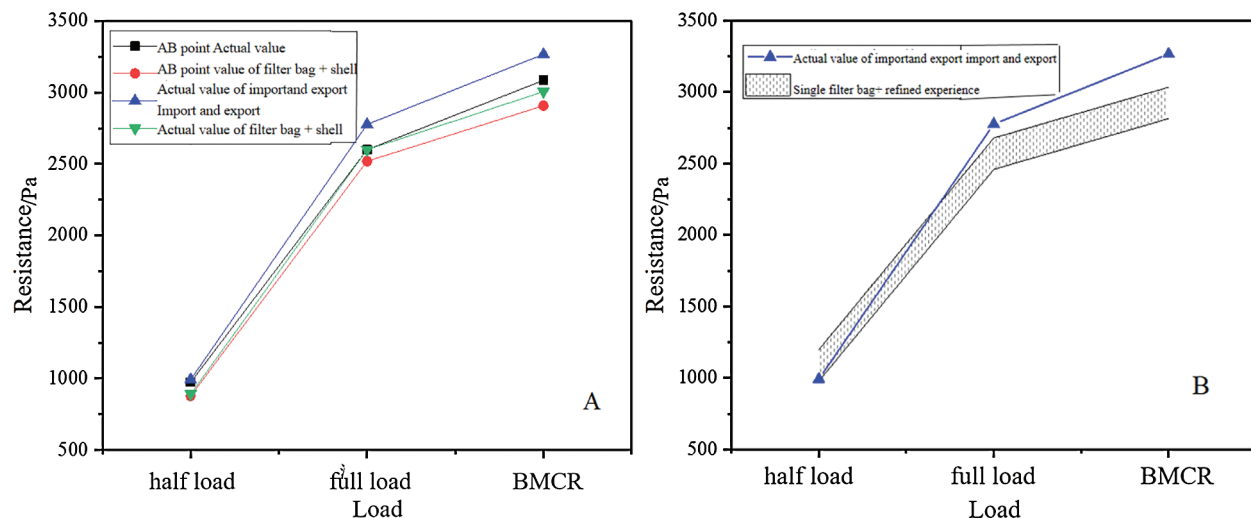


Figure 7: Statistics of the local simulation of the resistance of the bag filter and the measured value

$$P = (1 + \varepsilon) \cdot (np_B + p_S) \quad (9)$$

When using Method 3, only the pressure between the inlet and outlet can be obtained because the refined empirical values correspond to the shell of the bag filter. As shown in Fig. 7B, Method 3 can only be used to estimate the overall resistance of the bag filter in a wide range. However, because the empirical value is refined, the error range with respect to the resistance range and the actual measured value is kept below 17%, which satisfies the requirements of practical engineering prediction [28,29].

The comparison of the three methods demonstrates that the results of Method 1 are the most accurate; however, its complexity and consumption of time and calculation resources are the highest. Method 3 saves the most time and calculation resources by adding the refined experience value and the local simulation value; however, a large error is associated with its results. Thus, Method 3 is only applicable to practical engineering estimation. In Method 2, the maximum error is greater by only 1.1% when compared with that in Method 1; furthermore, its required time and calculation resources are relatively small. Thus, Method 2 is the optimal approach.

4.3 Analysis of the Internal Flow Field of Different Filter Bag Sizes

The ratio of the length of the filter bag to the radius is defined as the length–diameter ratio to reduce the resistance of the filter bag and the overall resistance of the bag filter. Using the original filter bag (65×8065 mm), only a single filter bag with different length–diameter ratios is simulated using Method 2. Because of the limitation of the overall size of the actual bag filter, the maximum filter bag radius can be increased by four times and the length–diameter ratio can be decreased by 2.25, 46.25, 912.25 and 14 times when maintaining the filtering area constant. The simulation is conducted under the most representative BMCR condition. Fig. 8 shows the plots of the static pressure and velocity of the shaft centre of the filter bag. In the figure, the upper part is the outlet, the lower part is the bottom of the filter bag, the right side is the windward side (inlet) and the left side is the leeward side. The static pressure plot shows that the pressure difference decreases with the decreasing length–diameter ratio. When the length–diameter ratio is decreased by nine times, the variation of the static pressure difference can no longer be distinguished at the same scale. Thus, the variation of the static pressure difference becomes small after the scale is reduced again. The velocity plot shows that with the decreasing length–diameter ratio, the rate of velocity change decreases and the tip of the velocity centre tends to become negligible.

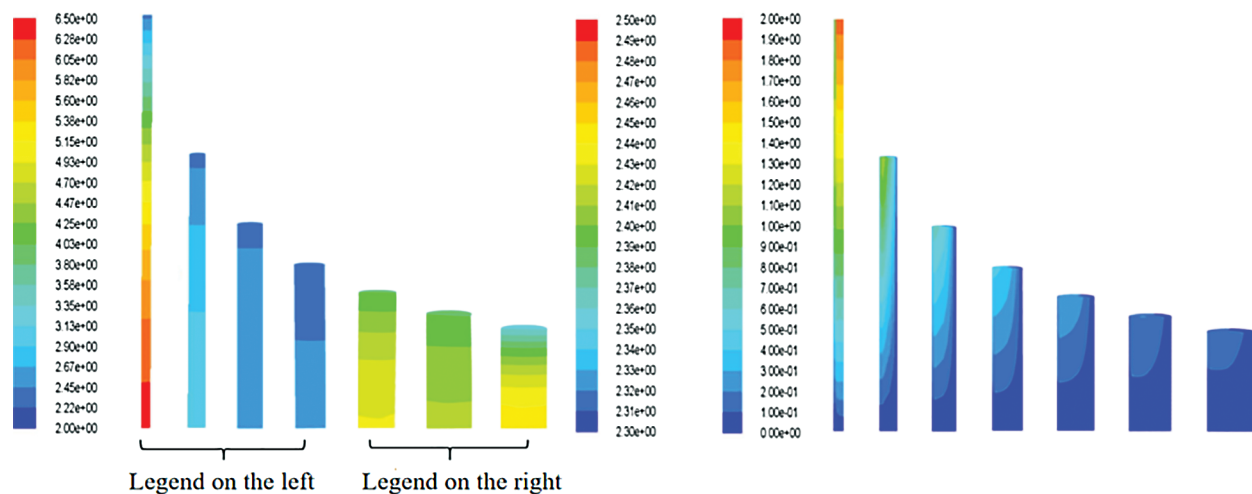


Figure 8: Plots of the static pressure and velocity of the filter bag

Therefore, the service life of the filter bag must be improved and the blowing damage and deformation associated with the cage must be prevented to reduce the resistance that can be attributed to the filter bag of the bag filter. The smaller the length–diameter ratio of the filter bag, the more will be the internal flow field, the lower will be the resistance, the fewer will be the velocity centres and the longer will be the service life of the filter bag.

5 Conclusion

A single bag is simulated via CFD to simplify the numerical simulation of the overall resistance of the bag filter and analyse the characteristics associated with the velocity and pressure fields of the filter bag. The local simulation method and the local simulation plus refined empirical number method are proposed, and the following conclusions are obtained.

1. In Method 1, the error associated with the simulation of the bag filter is less than 9.1%. However, it is a time-consuming and laborious method.
2. In Method 2, a single filter bag is simulated locally and the resistance value of the shell is also considered. The obtained result is less than the real value, and the error is less than 10.2%.
3. The modified coefficient ε is 5.7%–10.2%; therefore, the results of the local simulation method (Method 2) are more accurate than those of the remaining methods.
4. The refined empirical values associated with the shell of the bag filter matched with the 200-MW units are generally between 368 and 588 Pa. The value range is decreased by 26.7% when compared with the common empirical value.
5. When a single filter bag is simulated locally and the refined empirical value is added, the overall resistance error becomes less than 17%, which can satisfy the requirements of practical engineering prediction.
6. Under identical conditions, the smaller the length–diameter ratio of the filter bag, the more even will be the internal flow field, the lower will be the resistance and the longer will be the service life of the filter bag.

Funding Statement: The author(s) received no specific funding for this study.

Conflicts of Interest: The authors declare that they have no conflicts of interest to report regarding the present study.

References

1. Zhao, M. H. (2018). *Experimental study on air distribution and pressure characteristics of porous plate in electrostatic precipitator (Ph.D. Thesis)*. Zhejiang University, China.
2. Lv, Y., Yang, J. (2020). The elaboration of flow resistance model for a bag filter serving a 200 MW power plant. *Fluid Dynamics & Materials Processing*, 16(4), 827–835. DOI 10.32604/fdmp.2020.010343.
3. Liu, W. T. (2018). Research on ultra-low emission transformation scheme of electric precipitator of thermal power unit. *Value Engineering*, 37(29), 167–169.
4. Duan, Z. Y., Su, H. T., Wang, F. Y., Zhang, L., Wang, S. X. et al. (2016). Distribution characteristics of mercury and emission factors of atmospheric mercury in Chongqing municipal solid waste incineration plant. *Environmental science*, 37(2), 459–465.
5. Ma, W. J. (2015). Analysis on the failure of the filter bag of the electrostatic precipitator. *Ningxia Electric Power*, 14(5), 66–70.
6. Kim, J. U., Hwang, J., Choi, H. J., Lee, M. H. (2017). Effective filtration area of a pleated filter bag in a pulse-jet in a bag house. *Powder Technology*, 12(6), 522–527.
7. Rachid, B., Aurélie, J., Sylvain, D., Gueraoui, K., Le C. et al. (2019). Influence of air humidity on particle filtration performance of a pulse-jet bag filter. *Journal of Aerosol Science*, 18(7), 1–9. DOI 10.1016/j.jaerosci.2019.01.002.

8. Lu, Y. X., Cai, J., Wang, Y. J., Huang, W. L. (2017). Structural optimization of bag filter based on two-phase flow. *Journal of Nanjing Normal University (Engineering Technology Edition)*, 17(1), 42–47.
9. Park, S., Joe, Y. H., Shim, J., Park, H., Shin, W. G. (2019). Non-uniform filtration velocity of process gas passing through a long bag filter. *Journal of Hazardous Materials*, 17(15), 440–447. DOI 10.1016/j.jhazmat.2018.10.098.
10. Andersen, B. O., Nielsen, N. F., Walther, J. H. (2016). Numerical and experimental study of pulse-jet cleaning in fabric filters. *Powder Technology*, 27(8), 284–298. DOI 10.1016/j.powtec.2015.12.028.
11. Nie, H. H. (2015). *Study on the filtration performance of superfine glass fiber needle punched composite filter material (Ph.D. Thesis)*. Qingdao University, China.
12. Geng, C. Y., Wang, X. F. (2018). Design of circulating heating system of garbage incineration desulfurization dust remover. *China Environmental Protection Industry*, 42(6), 44–46.
13. Yin, G., Li, W. B., Luo, B., Yuan, S. J. (2016). Optimization of nozzle diameter of bag filter. *Journal of Environmental Engineering*, 10(11), 6603–6607.
14. Hu, Z. G., Hu, M. Y., Chang, A. L. (2005). *Dedusting technology of thermal power plant*. Beijing: China Water Conservancy and Hydropower Press.
15. Li, W. T. (2018). *Study on Optimization of exhaust system and energy-saving operation of a 350 MW unit (Ph.D. Thesis)*. North China Electric Power University, China.
16. Hu, K., Hu, T. T., Ma, H. (2018). *Detailed explanation of ANSYS fluent example*. Beijing: Mechanical Industry Press.
17. Chen, P., Huang, K., Wang, F., Xie, W., Wei, S. et al. (2019). Simulation of heat and mass transfer in a grain pile on the basis of a 2D irregular pore network. *Fluid Dynamics & Materials Processing*, 15(4), 367–389. DOI 10.32604/fdmp.2019.07762.
18. Neffah, Z., Kahalerras, H., Fersadou, B. (2018). Heat and mass transfer of a non-newtonian fluid flow in an anisotropic porous channel with chemical surface reaction. *Fluid Dynamics & Materials Processing*, 14(1), 39–56.
19. Kumar, K. G., Manjunatha, S., Rudraswamy, N. G. (2020). MHD flow and nonlinear thermal radiative heat transfer of dusty prandtl fluid over a stretching sheet. *Fluid Dynamics & Materials Processing*, 16(2), 131–146. DOI 10.32604/fdmp.2020.0152.
20. Sabrina, N., Ghezal, A., Abboudi, S., Spiteri, P. (2018). A numerical study of the transitions of laminar natural flows in a square cavity. *Fluid Dynamics & Materials Processing*, 14(2), 121–135.
21. Tu, G., Song, Q., Yao, Q. (2017). Experimental and numerical study of particle deposition on perforated plates in a hybrid electrostatic filter precipitator. *Powder Technology*, 50(11), 143–153. DOI 10.1016/j.powtec.2017.08.021.
22. Pan, L., Yang, Y. Z. (2012). Numerical simulation of internal flow field of bag filter. *Journal of Environmental Engineering*, 6(8), 2750–2754.
23. Hu, M. Y., Lei, Y. Q. (2009). *Bag filter of coal-fired power plant*. Beijing: China Power Press.
24. Xiang, X. D. (2013). *Dedusting theory and technology*. Beijing: Metallurgical Industry Press.
25. Xu, X. D. (2017). *Practice and exploration of quality management in social environmental testing laboratory (Ph. D. Thesis)*. Suzhou University of science and technology, China.
26. Wu, J., Li, X. Y., Chen, B. M., Gao, L., Wang, R. X., et al. (2014). Construction of heat transfer coefficient model of external heat rotary kiln with large particles and low filling rate. *Journal of Agricultural Engineering*, 30(13), 256–262.
27. Geng, Y. Y. (2017). Analysis of waste gas monitoring and comprehensive evaluation of fixed pollution sources in oil field. *Petrochemical Technology*, 24(4), 284.
28. Meng, L. Y., Zhu, F. H., Yi, Y. P., Wang, D. G., Zhang, X. D. (2016). Study on the test method of ultra-low emission particles in coal-fired power plants. *China Power*, 49(10), 123–126.
29. Wang, W. C., Li, W. J., Xu, D. M., Li, Q. M. (2019). Runoff prediction based on Markov chain correction gm-bp model. *South to North Water Diversion and Water Conservancy Technology*, 17(5), 44–49.